ELSEVIER

Journal of Fluids and Structures 18 (2003) 595–612

JOURNAL OF FLUIDS AND STRUCTURES

www.elsevier.nl/locate/jnlabr/yjfls

Influence of upstream turbulence on the fluidelastic instability of a parallel triangular tube bundle

M. Rottmann*, K. Popp

Institute of Mechanics, University of Hannover, Appelstrasse 11 30167 Hannover, Germany

Received 17 July 2002; accepted 11 July 2003

Abstract

The stability boundaries of a single flexible tube in one of the first rows of a tube bundle can be highly dependent on the turbulence characteristics of the upstream flow. For certain bundle geometries, increased turbulence yields a stabilization of a flexible tube in the critical row. If this stabilization also occurs on the more realistic condition of a fully flexible bundle, it could be a useful effect with respect to applications. The flow rate in a heat exchanger could be increased or existing stability problems could easily be solved by inserting turbulence grids at the inlet instead of changing the entire tube bundle. Therefore, wind tunnel tests have been carried out with various flexible tubes in the tube bundle. The vibrations in the tube bundle have been carefully observed and measured by means of accelerometers. These investigations still show a significant stabilizing effect of increased upstream turbulence. For a better understanding of the observed effects some theoretical investigations on the stability behavior of a relatively simple "tube-in-channel-flow" model for a single flexible tube have been performed. Here, a stabilizing effect of a disturbed flow velocity has been found which is similar to the effect observed in the experiments.

1. Introduction

Flow-induced vibrations in heat exchanger tube bundles subjected to cross-flow can cause fatal damages that result in the shutdown of a plant and expensive repairs of the broken tubes. A review of the different mechanisms that excite tube vibrations is given by Weaver and Fitzpatrick (1988). In the present paper, fluidelastic instability is considered, which has the greatest destructive potential. It can lead to short-term failures because of the large amplitudes of vibration exceeding the fatigue limit. Other mechanisms like turbulent buffeting rather result in long-term failures, e.g., due to fretting wear in the contact areas of tubes and guide plates.

Fluidelastic instability appears in two different mechanisms: as fluid-damping-controlled instability (galloping) and as fluidelastic-stiffness-controlled instability. Depending on the configuration of the tube array and on the mass damping parameter, one of these mechanisms is dominant. A characteristic of galloping is that the tubes predominantly vibrate in cross-flow direction. The components of the fluid force proportional to the tube velocity lead to a negative total damping, which results in the instability. This instability also occurs if only one single flexibly mounted tube in an otherwise fixed array is investigated. In case of the fluidelastic-stiffness-controlled mechanism the instability results from coupling effects of several tubes in an array by the fluid. Here, the stability investigations always require a bundle with several flexible tubes.

*Corresponding author.
E-mail address: rottmann@ifm.uni-hannover.de (M. Rottmann).
URL: http://www.ifm.uni-hannover.de.

0889-9746/$ - see front matter © 2003 Elsevier Ltd. All rights reserved.
doi:10.1016/j.jfluidstructs.2003.07.013

Nomenclature

a	bar width of turbulence grid (m)
a_T	perturbation of flow channel area due to tube motion (m)
A	flow channel area (m)
A_0	mean flow channel area (m)
b	damping constant of tube mounting (Ns/m)
C_d	drag coefficient
d	tube outside diameter, $d = 80$ mm
D	damping factor, $D \approx \delta/2\pi$
f_1	first natural tube frequency (s^{-1})
F_y	fluid force on the tube in cross-flow direction (N)
h	resistance coefficient
k	spring rate of tube mounting (N/m)
K	Connors coefficient
ℓ	tube length, $\ell = 0.8$ m
L_x	length scale in x direction (m)
m	tube mass (kg)
p	Connors coefficient
P	tube pitch (m) pressure in flow channel (N/m^2)
s	mesh size of turbulence grid (m), flow channel coordinate (m)
s_a	length of attached flow region (m)
s_1	considered length of flow channel (m)
S_u	Strouhal number based on the upstream velocity
t	time (s)
Tu	turbulence intensity
u_i	upstream flow velocity in i direction (m/s), $i = x, y, z$
u_T	flow channel velocity perturbation due to tube motion (m/s)
$\bar{u}_i$	mean upstream flow velocity in i direction (m/s)
u'_i	upstream flow velocity perturbation in i direction (m/s)
U	gap velocity (m/s)
U_0	mean flow channel velocity (m/s)
U_∞	mean upstream flow velocity (m/s), $U_\infty = \bar{u}_x$
V_r	reduced gap velocity, $V_r = U/(f_1 d)$
$V_{r,cr}$	critical reduced gap velocity
x	coordinate in in-flow direction (m)
X	grid distance (m)
y	coordinate in cross-flow direction (m)
$\hat{y}_r$	reduced peak amplitude of vibration, $\hat{y}_r = \sqrt{2}\ddot{y}_{\mathrm{r.m.s.}}/((2\pi f_1)^2 d)$
$\bar{\beta}$	center position of attached flow region
δ	logarithmic decrement of damping
δ_r	mass-damping parameter
μ	tube mass per unit length including fluid added mass (kg/m)
ρ	fluid density (kg/m^3)
σ_i	standard deviation of u_i (m/s)
$\ddot{\varphi}$	angular acceleration about the x-axis (m/s^{-2})
$\hat{\Psi}$	phase angle of area perturbation
ω	circular vibration frequency (s^{-1})

For the description of the stability behavior of different tube arrays Connors diagrams are commonly used. The reduced gap velocity V_r,

$$V_r = \frac{U}{f_1 d}, \tag{1}$$

at the stability boundaries of a bundle are plotted as a function of the mass-damping parameter δ_r,

$$\delta_r = \frac{\mu\delta}{\rho d^2}. \tag{2}$$

Here, U is the velocity in the gap between the tubes, f_1 is the first natural frequency of the tube, d is the tube outside diameter, μ is the mass per unit length including the fluid added mass, δ is the logarithmic decrement of damping and ρ is the fluid density. Since a reliable determination of stability boundaries based on theoretical models is not possible so far, the experimental investigation of the stability behavior of different bundle arrays is required. Experimental data from different researchers have been compiled to obtain the Connors equation,

$$V_{r,cr} = K\,(\delta_r)^p, \tag{3}$$

for the computation of the critical reduced gap velocity $V_{r,cr}$, which is essential for the heat exchanger design, see, e.g., Schröder and Gelbe (1999).

Fig. 1 from Austermann and Popp (1995) shows an example for an experimentally determined Connors diagram for a parallel triangular bundle with a pitch-to-diameter ratio $P/d = 1.375$. Investigated were the vibrations of one single flexible tube in the first four rows of an otherwise rigid bundle. The different markers used for the stability boundaries in Fig. 1 indicate the different positions of the flexible tube in the bundle, in accordance with the sketches in the diagram. Clearly, the third tube row is the critical one with lowest critical reduced gap velocity and a large unstable region in the δ_r, V_r-plane. At low mass-damping parameters smaller unstable regions were also found for the tube in the second and fourth row. Furthermore, Austermann and Popp (1995) found that the stability boundaries of a single flexible tube in the parallel triangular and also in the in-line square configuration agree well with stability boundaries of the fully flexible bundles, i.e., the galloping mechanism is dominant here. As a matter of fact it is always one of the first rows of these tube bundles that is the critical one. Here the turbulence intensity in test tube bundles is usually low. The stability behavior improves downstream inside the bundle where the turbulence is generated by the bundle itself.

This led to the question of whether the stability behavior in the first rows is different with a more turbulent flow at the inlet of the bundle. Therefore, the influence of upstream turbulence on the stability behavior of a single flexible tube in the critical row of an otherwise fixed bundle has already been investigated in recent years. For the definition of the parameters used for the description of the upstream turbulence see the corresponding chapter below. For a tube in the critical third row of the parallel triangular bundle Romberg and Popp (1996) have shown, that the large region with unstable tube behavior in the 'δ_r, V_r'-plane at undisturbed flow has completely vanished at a higher level of upstream turbulence. Later the transition from the unstable to the stable behavior was found by increasing the turbulence intensity in small steps, cf. Fig. 2 taken from Rottmann and Popp (2001). Here, the nondimensional amplitude $\hat{y}/d$ of the tube in cross-flow direction is plotted versus the reduced gap velocity V_r for a constant mass-damping parameter. With increasing turbulence intensity Tu the unstable region along the velocity-axis becomes smaller and the amplitudes of the vibrations decrease until a complete stabilization is reached. In the present study the investigations of the stability behavior are extended to bundles with various flexible tubes.

Other experimental investigations of the subject can be found in Southworth and Zdravkovich (1975), Gorman (1980) and Soper (1982). Southworth and Zdravkovich (1975) investigated the vibrations of one and two flexible tube rows in a wind tunnel. Grids that were introduced upstream of the tube rows caused a significant change of the tube behavior. In particular for large transverse pitch-to-diameter ratios ($P/d = 2$) there was no sudden rise of the amplitudes at a certain critical flow velocity as observed in the experiments without grid. Gorman (1980) tested the behavior of normal triangular and in-line square bundles ($P/d = 1.36, .., 1.48$) in water cross-flow. In many cases the amplitudes of vibration were significantly lowered by introducing different screens or grids. Soper (1982) found that turbulence can either increase or decrease the critical flow velocity for the fluidelastic instability of a normal triangular bundle in air cross-flow ($P/d = 1.25$). Thus, stabilizing effects due to turbulence grids have been found by different researchers. However, the results are not suitable for a direct comparison, since the authors have investigated different configurations (different bundle geometries, air or water cross-flow) and turbulence characteristics have not been determined.

Furthermore, several theoretical models for the computation of tube bundle vibrations can be found in the literature. A review of the different models published until 1993 is given by Price (1995). Among other models there are semi-analytical models using a simplified fluid mechanics approach. One of these models is the "tube-in-channel-flow" model, which was originally published by Lever and Weaver (1982) and extended many times (e.g., Lever and Weaver, 1986; Rzentkowski and Lever, 1992). This model is also taken as a basis for the theoretical considerations of the influence of turbulence on the stability behavior in this paper. In addition to the models reviewed by Price (1995) CFD-Codes combined with a model for the structure should be mentioned here. The comparison of vibration measurements and simulations by Kassera and Strohmeier (1997) proves that good results have been obtained in recent years. Here,

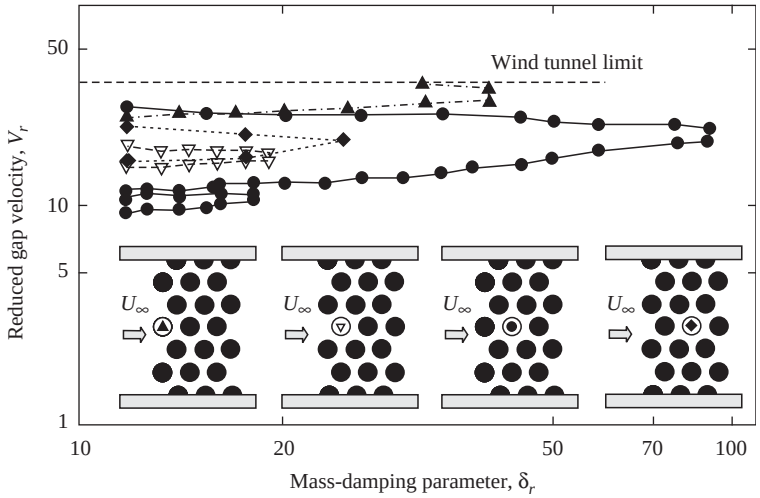

Fig. 1. Stability diagram for one flexibly mounted cylinder in an otherwise rigid parallel array, $P/d = 1.375$ (Austermann and Popp, 1995).

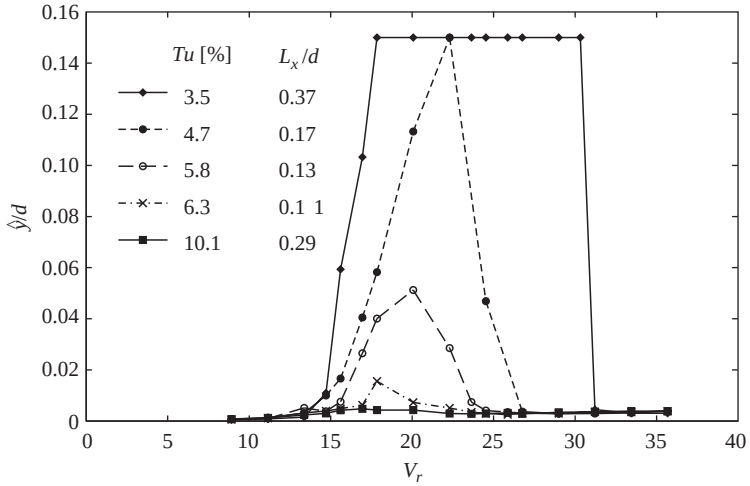

Fig. 2. Transition from unstable to stable behavior with increasing turbulence intensity, parallel triangular bundle, $P/d = 1.375$, 3rd row, $\delta_r = 15$ (Rottmann and Popp, 2001).

the sensitivity of the stability behavior with respect to changes of the turbulence characteristics could be included in the investigations.

2. Experimental set-up

A picture of the tube bundle test rig can be seen in Fig. 3. The rig is placed in a wind tunnel test section where the tube bundle is exposed to air cross-flow. The test rig was originally developed by Austermann (1993) to investigate vibrations of a single flexible cylinder in otherwise fixed tube bundles. Therefore, one tube is mounted on springs outside the side walls. The springs are equipped with strain gauges to measure the displacements. The damping is adjustable by means of eddy current dampers. Computer-controlled adjustable mounts allow to maintain the ideal bundle geometry at any fluid velocity, independent of the static displacement. The sidewalls of the apparatus were designed to mount different

patterns of rigid tubes around the flexible cylinder. For the investigations presented in this study an extended setup has been used, where the rigid tubes could be substituted by flexible ones.

The mounting of these flexible tubes can be seen in the picture of a sliced tube in Fig. 4. The mounting is identical at both ends of the tube, arranged symmetrical to the tube center. Respectively, one end of a circular spring is clamped in a sidewall mounting, which can be fixed at the sidewall by a screw. The other end is clamped in a cross-spring unit that is fastened in the tube. The cross-spring unit is soft in axial direction for the limitation of the axial forces to obtain a linear spring characteristic. The springs have the same total spring rate like those of the existing flexible tube and a weight has been fastened in the tube center to obtain the same mass. It should be noted that such a tube has four rigid body modes of vibration, namely two translational modes in cross-flow direction and in in-flow direction with the same natural frequency f_1 and two corresponding rocking modes with a natural frequency f_2.

In preliminary investigations the structural damping of the new tubes have turned out to be smaller than the structural damping of the existing tube. Because of that the existing tube has not been used for the vibration measurements in this study. It has been placed in the first row and tubes with smaller structural damping are mounted in the critical third row. The vibrations of one of the tubes in the third row are measured by means of four accelerometers, two of them at each end of the tube, see also Fig. 3, so that the four rigid body modes of vibration can be distinguished.

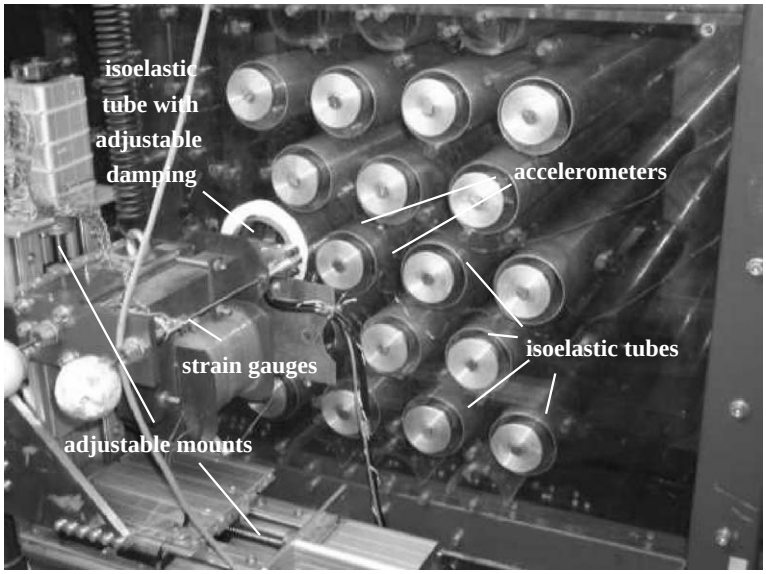

Fig. 3. Parallel triangular bundle, $P/d = 1.375$.

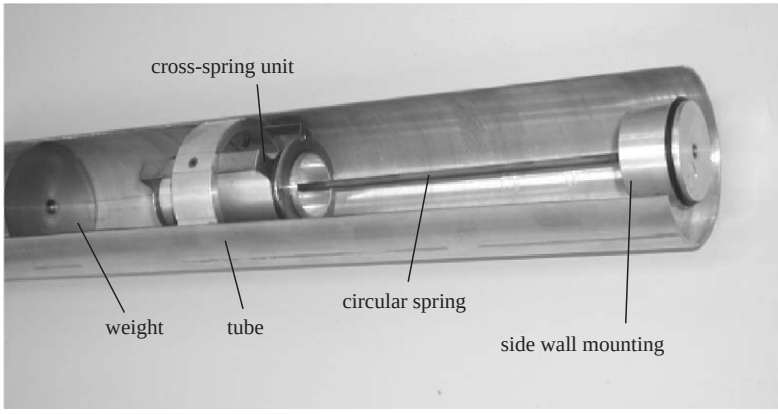

Fig. 4. Tube mounting.

The different configurations of flexible and rigid tubes investigated in this study are shown in Fig. 5. The bundle always consists of 18 tubes in seven rows. The numbered tubes are the flexibly mounted ones, respectively. Here, tube 1 is the old tube with the adjustable mounts outside the sidewalls and tube 2 is the tube in the third row that is equipped with accelerometers for vibration measurements. In tube bundle A one single tube is flexible in the otherwise rigid bundle. This was investigated again to show the effect of turbulence on the behavior of this tube with lower structural damping. In bundle B only tube 2 and its neighbors in the second and first row are flexible. Tube bundle C contains three fully flexible lines with 10 flexible tubes and bundle D is the fully flexible bundle with 18 flexible tubes.

All tubes have an outside diameter of $d = 80$ mm and a length of $\ell = 800$ mm. The tube masses are $m_1 = 2.77$ kg for tube 1 and $m_i = 2.7$ kg for the tubes 2–18. The other structural parameters of the tubes were obtained by tests of free oscillations, which where evaluated using a software tool for vibration analysis, cf. Fig. 6. The results for the natural frequencies, logarithmic decrements of damping and mass-damping parameters can be found in Table 1. The small differences of the natural frequencies $f_{1,i}$ of the translational modes, which are all within a limit of $\Delta f_{1,i}/\bar{f}_{1,i} < 1\%$, are probably due to small differences of the spring lengths. Differences of the logarithmic decrements δ_i of damping can be explained with different friction characteristics in the clamps.

Unlike in the former investigations of the single flexible tube, see Austermann (1993), Austermann and Popp (1995), Romberg and Popp (1996), Rottmann and Popp (2001), some deviations from the ideal bundle geometry must be accepted with this set-up. To determine geometry deviations in the in-flow direction, the static displacements have been measured for the flow velocity $V_r \approx 25$ which is the maximum velocity investigated in the flexible bundles. It was found, that the static displacement in flow direction in the first row is about 1 mm, in the third row about 0.5 mm. In the worst case that results in a deviation of the gap area between these tubes of about 1.7% from the ideal geometry, i.e., these deviations are considered to be small. In cross-flow direction the displacement of the flexible tubes due to gravity is about 3 mm. This has no effect in the fully flexible bundle (bundle D) where all tubes have the same static displacement. However, it must be considered that the displacements can affect the behavior of the other bundles, where the gap areas between flexible and rigid tubes differ from the ideal value by about 8.6%.

3. Description and generation of turbulence

For the description of a turbulent flow field statistical methods are commonly used, although they give no insight in the underlying mechanisms (e.g., Landahl and Mollo-Christensen, 1992). The flow field can formally be described by three velocity components and three cartesian coordinates,

$$\mathbf{u} = \mathbf{u}(\mathbf{x}, t), \quad \mathbf{u} = (u_x, u_y, u_z)^{\mathrm{T}}, \quad \mathbf{x} = (x, y, z)^{\mathrm{T}}. \tag{4}$$

Here, the single velocity components can be written as the sum of the mean value $\bar{u}_i(\mathbf{x})$ and the fluctuating part $u_i'(\mathbf{x}, t)$.

$$u_i(\mathbf{x}, t) = \bar{u}_i(\mathbf{x}) + u_i'(\mathbf{x}, t), \quad i = x, y, z. \tag{5}$$

A common assumption for the flow field is a normal distributed stationary velocity process. Then the velocity distribution is well-defined by the mean value $\bar{u}_i$ and the standard deviation σ_i. Further assuming an ergodic process the two values can be obtained from a sufficient long averaging in time,

$$\bar{u}_i(\mathbf{x}) = \lim_{T \to \infty} \frac{1}{T} \int_0^T u_i(\mathbf{x}, t)\, \mathrm{d}t, \tag{6}$$

$$\sigma_i^2(\mathbf{x}) = \lim_{T \to \infty} \frac{1}{T} \int_0^T [u_i(\mathbf{x}, t) - \bar{u}_i(\mathbf{x})]^2\, \mathrm{d}t. \tag{7}$$

Combining these two values for a flow with the main flow direction x the turbulence intensity Tu as one turbulence parameter can be defined

$$\mathrm{Tu} = \frac{\sigma_x}{\bar{u}_x}. \tag{8}$$

Furthermore, the flow states in the motion of a continuum are correlated in space and time. Mathematically the similarity of the flow states with an offset in space and time can be described by the correlation function in the general formulation

$$R_{ij}(\mathbf{x}, \mathbf{r}, \tau) = \overline{u_i'(\mathbf{x}, t)\, u_j'(\mathbf{x} + \mathbf{r}, t + \tau)}, \quad i, j = x, y, z. \tag{9}$$

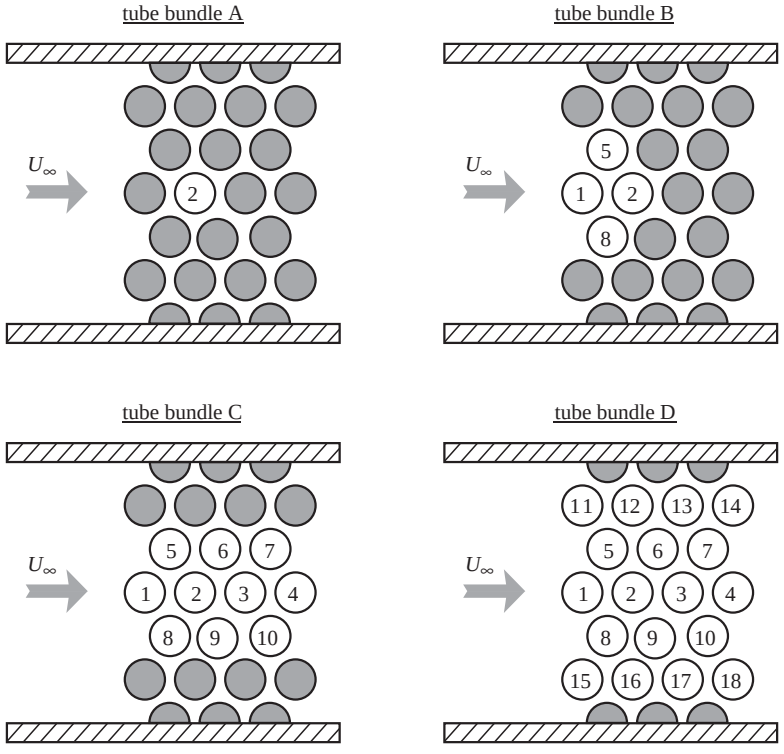

Fig. 5. Sketch of investigated tube bundles.

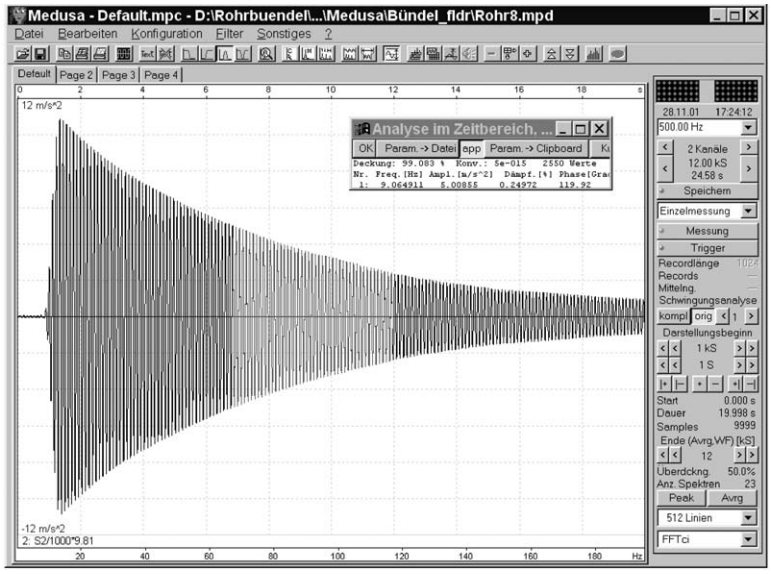

Fig. 6. Test of free oscillations.

Here, $\mathbf{r}$ is the offset vector and τ is the offset time. From the correlation function the length scales

$$L_{ij,k} = \frac{1}{2\sqrt{R_{ii}(\mathbf{x},0,0)\,R_{jj}(\mathbf{x},0,0)}} \int_{-\infty}^{\infty} R_{ij}(\mathbf{x}, r_k, 0)\,\mathrm{d}r_k, \quad k = x, y, z, \tag{10}$$

can be calculated as an information about the spatial character of the flow field. A characteristic parameter, which describes the average length of a turbulence eddy, is the length scale $L_x = L_{xx,x}$ for two velocity components and an

Table 1
Structural tube parameters

Tube no. i	Natural frequency $f_{1,i}$ (Hz)	Damping factor D (%)	Mass damping parameter $\delta_{r,i}$
1	8.90	0.53	14.78
2	8.92	0.26	7.25
3	8.94	0.17	4.74
4	9.01	0.25	6.97
5	8.88	0.25	6.97
6	8.91	0.20	5.57
7	9.07	0.24	6.69
8	9.03	0.18	5.02
9	8.89	0.25	6.97
10	9.01	0.22	6.14
11	8.96	0.19	5.30
12	8.95	0.17	4.47
13	9.04	0.25	6.97
14	8.90	0.26	7.25
15	8.97	0.27	7.53
16	9.03	0.26	7.25
17	8.99	0.23	6.41
18	9.01	0.22	6.14

offset vector in the main flow direction. In a homogeneous flow field the correlation function is even and the length scale is independent of the position vector $\mathbf{x}$. Then L_x can be determined at an arbitrary position $\mathbf{x}_0$ by

$$L_x = \frac{1}{\sigma_x^2(\mathbf{x}_0)} \int_0^\infty R_{xx}(\mathbf{x}_0, r_x, 0)\, \mathrm{d}r_x. \tag{11}$$

To vary the turbulence characteristics at the inlet of the bundle, turbulence grids were placed in the test-section, cf. Fig. 7. For the experimental determination of the turbulence parameters, time series of the flow velocity have been measured by means of hot-wire anemometers in a plane in front of the bundle inlet. In these experiments the assumptions of Gaussian distributed velocity fluctuations and a homogeneous turbulence field are confirmed well. The characteristics found in the turbulence investigations agree well with the results of other authors who investigated the flow behind grids (e.g., Baines and Peterson, 1951). The turbulence parameters are largely independent of the mean-fluid velocity U_∞ in the considered parameter region. However, the grid distance X, the mesh size s, the bar width a, the geometry of the bars and the tube bundle itself have an influence on the turbulence intensity Tu and the length scale L_x. Using different turbulence grids with various distances X turbulence intensities between Tu = 3.5% and 23% have been generated at the inlet of the bundle. Some more details about the experimental flow field investigations can be found in Romberg and Popp (1996).

4. Stability behavior

To discuss the influence of the different static deflections on the critical velocity, the vibration behavior of the different bundles in a flow with low upstream turbulence, Tu = 3.5%, can be compared. Fig. 8 shows the reduced amplitudes $\hat{y}_r$ in cross-flow direction of tube no. 2 in the critical third row of the different tube bundles. From measured time series of the acceleration $\ddot{y}$ the reduced amplitudes $\hat{y}_r$ have been computed by

$$\hat{y}_r = \frac{\sqrt{2}\, \ddot{y}_{\mathrm{r.m.s.}}}{(2\pi f_1)^2\, d}. \tag{12}$$

In case of a harmonic tube motion this value is the peak amplitude of vibration divided by the tube diameter d. The measurements were stopped at a certain amplitude, when the tube impacts against the mechanical stops. The behavior of the tube bundles B, C and D with 4, 10 and 18 flexible tubes is the same. The amplitudes of vibration suddenly increase at a critical reduced gap velocity of about $V_{r,cr} \approx 11$. Furthermore, the third row turned out to be the critical one indeed, which starts to vibrate at large amplitudes first. Since this behavior is identical, the authors believe that the

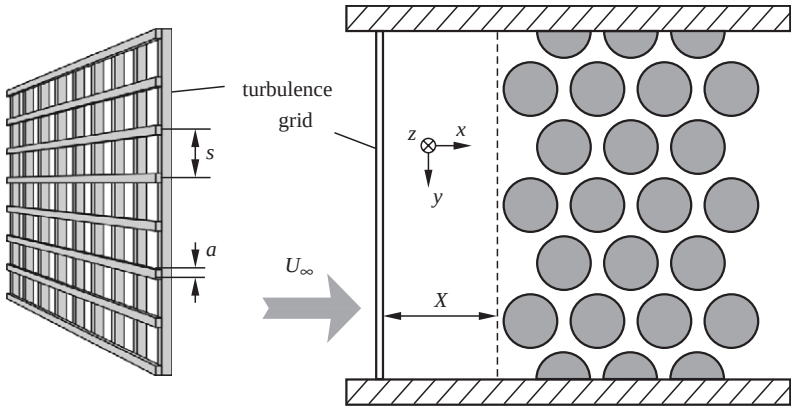

Fig. 7. Experimental set-up for increasing the turbulence at the inlet of the tube bundle.

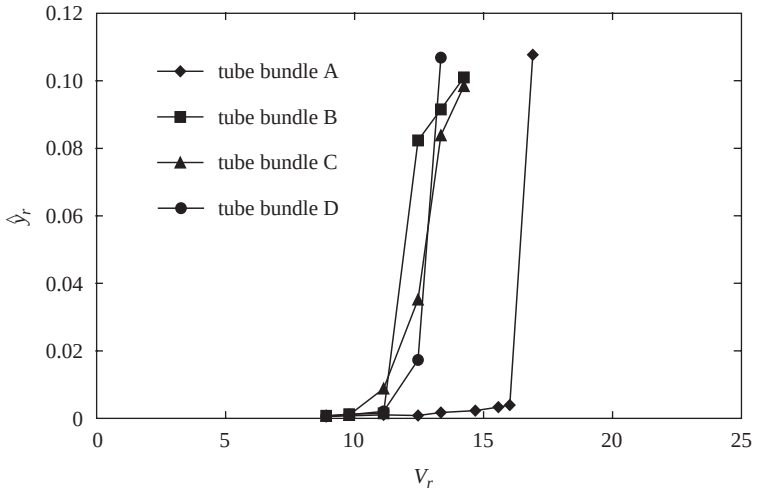

Fig. 8. Reduced amplitudes of tube no. 2 in cross-flow direction for different test cases, Tu = 3.5%.

different static displacements do not play an important role for the stability behavior of these three bundles. However, the critical value of V_r is higher for tube bundle A ($V_{r,cr} \approx 16$). Here, the authors believe, that this is due to the static displacement, that solely occurs at the single flexible tube but not at the neighbors. This behavior agrees well with the observations of Austermann (1993) who found, that shifting the equilibrium position of the single flexible tube in cross-flow direction led to slightly increased critical velocities. Therefore, tube bundle A should be considered as a particular test case with deviations from the ideal bundle geometry, whereas these deviations can be neglected for the other test cases.

It should also be noted that the vibrations depicted in Fig. 8 are due to fluidelastic instability and not a result of vortex shedding. The critical reduced gap velocity for the tube bundles B, C and D of about $V_{r,cr} \approx 11$ corresponds to an upstream velocity $U_\infty = 2.5$ m/s. For this array the expected Strouhal number S_u based on the upstream velocity is $S_u \approx 1.5$ (e.g., Weaver et al., 1986). This yields an expected vortex shedding frequency $f_v = S_u U_\infty / d = 46.8$ Hz, which is far removed from the natural frequency of the test tube ($f_{1,2} = 8.92$ Hz).

Looking at the influence of upstream turbulence on the stability behavior the stabilizing effect is confirmed well in the particular case of a single flexible tube, cf. Fig. 9. For low turbulence intensities a lower and an upper stability boundary is found within the investigated velocity range. The critical reduced gap velocity for Tu = 3.5% is about $V_{r,cr} \approx 16$. With increasing turbulence intensities particularly the upper stability boundary moves to smaller reduced gap velocities V_r. The peak amplitudes of vibration decrease with increasing turbulence intensity and at a value of Tu = 13.8% the equilibrium position of the tube is stable all investigated velocities. This agrees very well with the behavior in a bundle with ideal geometry described in Rottmann and Popp (2001), cf. Fig. 2.

The stability behavior of the bundles with various flexible tubes at increased upstream turbulence turned out to be more complex. For tube bundle B with four flexible tubes, see Fig. 10, a stabilization with increasing turbulence intensity is found in the region $V_r \leqslant 20$. However, at a velocity of $V_r \approx 21$ the tube motion reaches a stability boundary despite the increased turbulence. The observation was that the first and the second row are the ones with the largest amplitudes here. The measurements were stopped at a velocity $V_r = 22.3$ because the vibrations of a tube in the second row reached the mechanical stop. Therefore, the velocity range investigated for this bundle is smaller then the range investigated for bundle A with one single flexible tube. To specify the motions beyond the stability boundaries the acceleration $\ddot{y}$ in cross-flow direction is plotted versus the acceleration $\ddot{x}$ in in-flow direction for two turbulence intensities in Fig. 11. At a low turbulence intensity, where the instability of the array is governed by the tube in the third row, it is predominantly a motion in cross-flow direction which is also known from the single flexible tube in the third row. At a higher turbulence intensity, where the amplitude of the other tubes are higher, a tube in the third row rather moves on an elliptic trajectory, supposably due to coupling effects with the other tubes.

The influence of turbulence on the stability behavior of the tube bundles C and D with more flexible tubes is a bit different from bundle B, cf. Figs. 12 and 13. At an increased turbulence intensity of Tu = 10.1% no significant change in the vibration behavior has occurred. At further increased turbulence intensity of Tu = 13.8% the stability behavior of the arrays improve to critical values of the reduced gap velocity $V_{r,cr} > 15$. The behavior of the two configurations is very similar here. In both bundles, tubes from the second to the fourth row vibrate at large amplitudes. From the observations it is impossible to decide if there is one critical row at the onset of the instability. The measurements were stopped at a velocity $V_r = 22.3$ because the amplitudes of some tubes occasionally exceeded the clash limit with the stops. Finally, at the highest investigated turbulence intensity, Tu = 23%, a different behavior of the bundles C and D was found. Bundle C becomes unstable in the translational mode of vibration at $V_r \approx 17.5$, cf. Fig. 12. For tube bundle D no abrupt rise of the reduced amplitude which indicates a stability boundary was detected in the investigated velocity range, cf. Fig. 13.

Nevertheless tube bundle D also reaches a stability boundary here. In Fig. 14 the r.m.s. value $\ddot{\varphi}_{\mathrm{r.m.s.}}$ of the angular acceleration about the x-axis, the rocking mode of vibration with the eigenfrequency $f_2 = 17.2$ Hz, is plotted versus the reduced gap velocity (V_r based on the natural frequency f_1) for the turbulence intensities Tu = 13.8% and 23%. At a velocity $V_r \approx 17.5$ the r.m.s.-value sharply increases for the higher turbulence intensity Tu = 23%. It seems that turbulence, which is the only characteristic varied in the Figs. 13 and 14, transfers the instability to the rocking mode of vibration. At the onset of this instability the largest amplitudes of the rocking second mode were not observed at the monitored tube but at a tube in the second row.

To illustrate the different kind of instability the probability density functions of measured time series are plotted in the Figs. 15 and 16. Fig. 15 shows the probability densities of the translational acceleration $\ddot{y}$ and the angular acceleration $\ddot{\varphi}$ at a reduced gap velocity $V_r = 22.3$ and the lower turbulence intensity Tu = 13.8%. The density function of $\ddot{y}$ has a minimum in the center and two excentric peaks. This kind of probability density is typical for a limit cycle motion with a superimposed stochastic perturbation. The density function of $\ddot{\varphi}$ is similar to a Gaussian distribution, which indicates a random vibration of a stable mode. These characteristics have interchanged at the same reduced gap velocity but higher turbulence intensity Tu = 23%, see Fig. 16. Here, the translational mode performs randomly distributed vibrations and the distribution of the angular acceleration characterizes a limit cycle motion with perturbations.

5. Discussion of the experimental results

The behavior of a tube bundle can significantly change when turbulence parameters are varied. For a single flexibly mounted tube in a fixed array the stabilizing effect of upstream turbulence reported earlier has been confirmed. In the other investigated cases of 4 and 10 flexible tubes and also in case of a fully flexible bundle the stability boundary is shifted to higher values with increasing turbulence intensity. Of course, this results in increased amplitudes due to buffeting.

When only the vibrations of one tube are measured it cannot be decided whether the galloping instability of a particular tube or a coupling mechanism causes the instability of the array. Nevertheless it is a remarkable observation, that the instabilities in the flexible bundles at high turbulence intensities were rather triggered by vibrations of the second and fourth row, because also Austermann and Popp (1995) found instabilities of a single tube in these rows for low mass damping parameters, cf. Fig. 1. Here, it seems possible that already a slightly increased structural damping could suppress these instabilities. Then the stabilization due to turbulence could still gain more relevance for the behavior of the bundle.

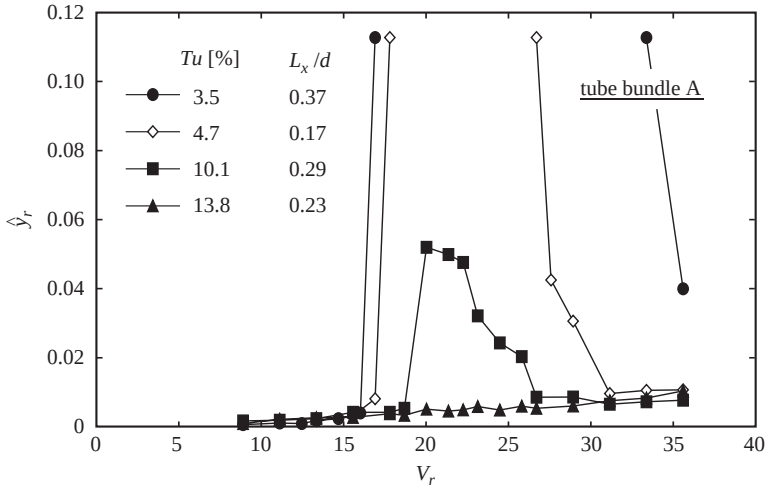

Fig. 9. Reduced amplitudes of tube no. 2 in cross-flow direction, tube bundle A.

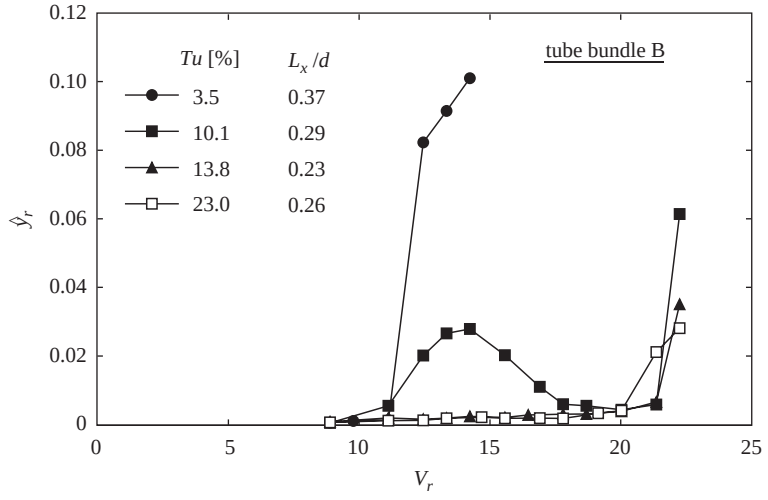

Fig. 10. Reduced amplitudes of tube no. 2 in cross-flow direction, tube bundle B.

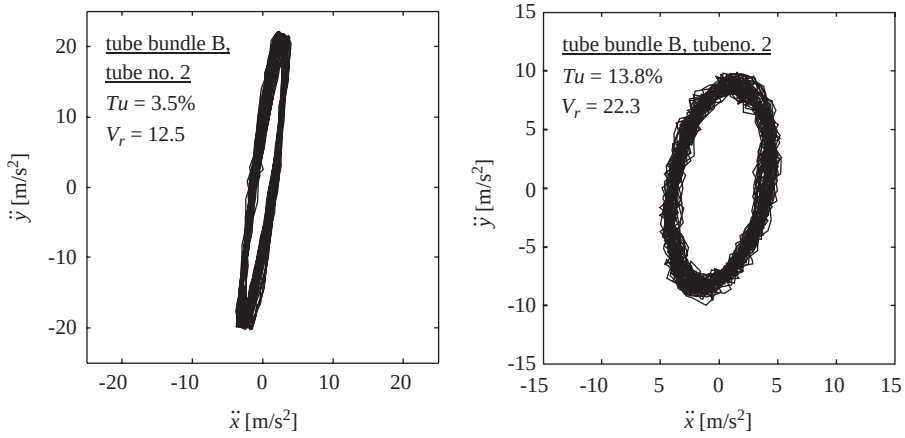

Fig. 11. Tube motion at low and high turbulence intensity.

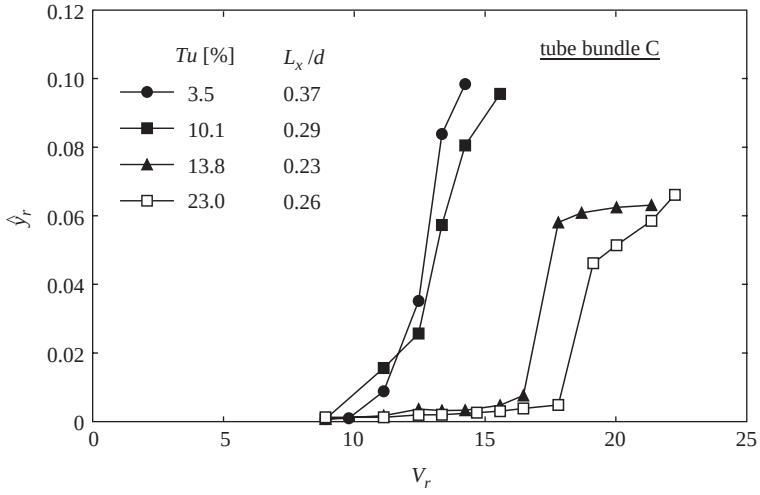

Fig. 12. Reduced amplitudes of tube no. 2 in cross-flow direction, tube bundle C.

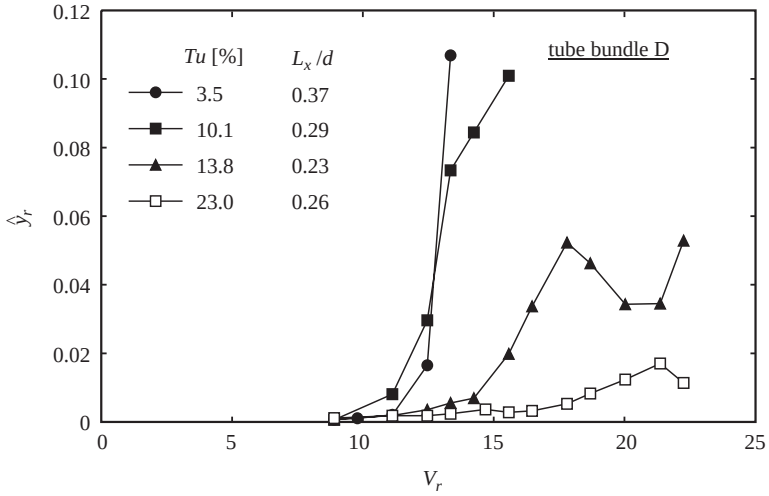

Fig. 13. Reduced amplitudes of tube no. 2 in cross-flow direction, tube bundle D.

For the fully flexible bundle it is astonishing that at high turbulence intensities the rocking mode of vibration becomes critical. Here, the authors believe that this mode cannot represent the second mode of a real tube because of the design of the tube mounting with springs inside the tubes and a mass in the tube center. This results in a low torsional spring constant and a low mass moment of inertia for this mode of vibration.

However, this mode switching could be interesting from the scientific point of view. In the literature stabilizing effects of turbulence have been found by Bucher and Lin (1988) in theoretical investigations in the related field of bridge structures under turbulent wind. A stabilization of an unstable mode occurs provided that an appropriate coupling with other modes, which become less stable, exists. In the mathematical literature Arnold (1990) reports on a stabilization of linear systems by noise in the system matrix. A stabilization is possible, if the sum of the eigenvalues is negative. Since this sum is positive for an unstable one degree of freedom system, this means that coupled modes are necessary for the stabilization.

6. Theoretical considerations

The theoretical considerations are based on the tube-in-channel-flow model for fluidelastic instability which was first published by Lever and Weaver (1982). A basic assumption is that the flow through the tube bundle is a flow in

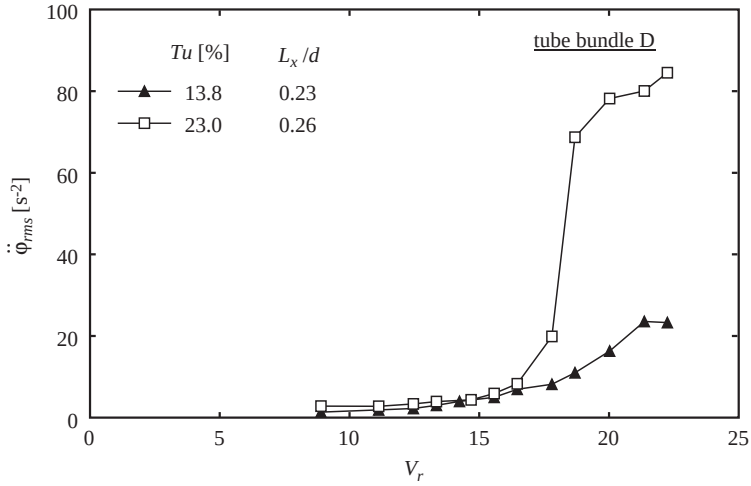

Fig. 14. Angular acceleration about x-axis, tube bundle D.

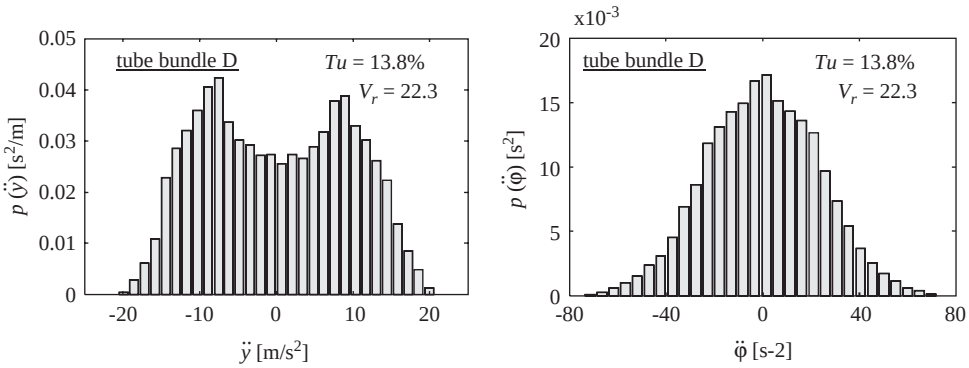

Fig. 15. Probability density functions of $\ddot{y}$ and $\ddot{\varphi}$.

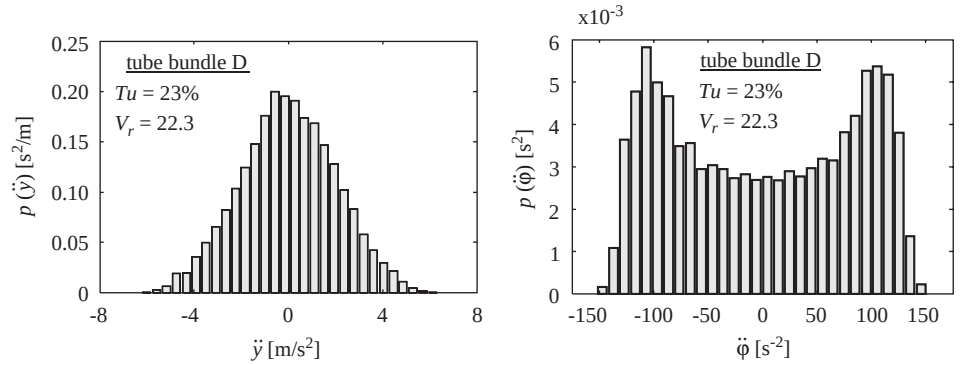

Fig. 16. Probability density functions of $\ddot{y}$ and $\ddot{\varphi}$.

unconnected channels, see Fig. 17. The flow through these channels is described by one-dimensional stream line theory. The channel area $A(s,t)$ depends on the bundle geometry and on the tube motion. This is considered in the general approach

$$A(s,t) = A_0 + a_T(s,t). \tag{13}$$

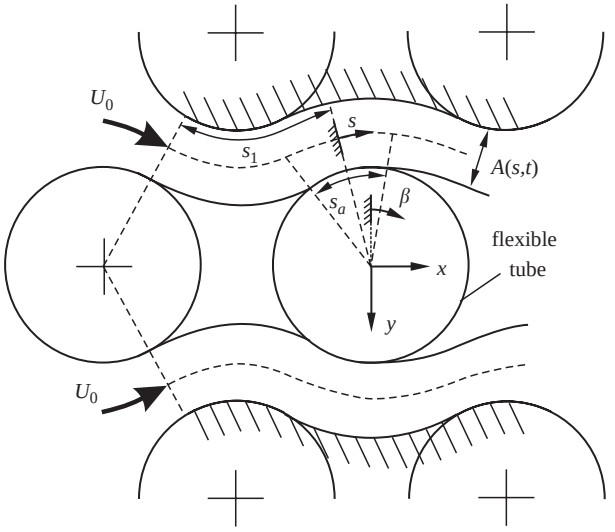

Fig. 17. Flow channels in a parallel triangular tube bundle.

Here, A_0 is the area in the rigid bundle and $a_T(s,t)$ is a small perturbation due to the tube motion, which is specified below. Similarly, for the flow velocity $U(s,t)$ in a channel it is assumed that

$$U(s,t) = U_0 + u_T(s,t), \tag{14}$$

where $u_T(s,t)$ is a small velocity perturbation that results from the tube motion. Using the continuity equation

$$\int_{-s_1}^{s} \frac{\partial a_T(s,t)}{\partial t}\,\mathrm{d}s + A(s,t)U(s,t) = A(-s_1,t)U(-s_1,t), \tag{15}$$

the velocity perturbation $u_T(s,t)$ can be computed. Subsequently, the relation between the velocity distribution $U(s,t)$ and the pressure distribution $P(s,t)$ is obtained applying the Bernoulli equation

$$\frac{1}{\rho}P(s,t) + \frac{U^2(s,t)}{2} + \int_{-s_1}^{s} \frac{\partial U(s,t)}{\partial t}\,\mathrm{d}s + \frac{h}{2s_1}\int_{-s_1}^{s} U^2(s,t)\,\mathrm{d}s = \frac{1}{\rho}P(-s_1,t) + \frac{U^2(-s_1,t)}{2}. \tag{16}$$

Neglecting small second-order terms the equations can be solved and finally the approximation

$$F_y(t) = s_a \ell \cos\bar{\beta}(P_1(0,t) - P_2(0,t)) \tag{17}$$

is used for the fluid force on the tube in y direction. The origin of the channel coordinate is chosen in the center of the attached flow region, s_a is the length and the angle $\bar{\beta}$ denotes the center position of this region ($\bar{\beta} = \beta(s=0)$), ℓ is the tube length and the indices 1 and 2 indicate the upper and lower flow channel in Fig. 17.

To define the above mentioned approach for the area perturbation $a_T(s,t)$ a harmonic tube motion in cross-flow direction, which is the main direction of motion, is assumed. At the position $s = 0$ in the center of the attached flow region the area perturbation of the upper channel results from the linearized channel geometry:

$$a_{T,1}(0,t) = \cos\bar{\beta}\, y(t) = \cos\bar{\beta}\, y_0 \cos(\omega t). \tag{18}$$

Then, it is assumed that this area perturbation also occurs upstream from the tube with a phase delay. The phase angle at the inlet is $\Psi(-s_1) = \hat{\Psi}$. Inside the channel the phase angle varies linearly from the center of the attached flow region to the inlet.

$$a_{T,1}(s,t) = \cos\bar{\beta}\, y_0 \cos\left(\omega t + \hat{\Psi}\frac{s}{s_1}\right). \tag{19}$$

In an analogous way, this approach for the lower channel yields

$$a_{T,2}(s,t) = -\cos\bar{\beta}\, y_0 \cos\left(\omega t + \hat{\Psi}\frac{s}{s_1}\right). \tag{20}$$

Now, the fluid force can be computed and inserted in the equation of motion.

$$\dot{m}\ddot{y} + (b + 0.5\rho C_d \ell d U_0)\dot{y} + ky = F_y(t). \tag{21}$$

For the stability analysis the fluid force is decomposed in terms proportional to the tube displacement $y(t) = y_0 \cos(\omega t)$ and to the tube velocity $\dot{y}(t) = -y_0\omega \sin(\omega t)$. This yields an equation of motion of the form

$$m\ddot{y} + \tilde{d}(U_0, \ldots)\dot{y} + \tilde{k}(U_0, \ldots)y = 0, \tag{22}$$

where the net damping constant $\tilde{d}(U_0, \ldots)$ depends on the undisturbed flow velocity U_0 and accordingly on the reduced gap velocity V_r. This term vanishes at the stability boundary and, thus, the mass-damping parameter of the stability boundary is obtained depending on the reduced gap velocity. Austermann (1993) identified the phase angle $\hat{\Psi}(V_r)$ of a tube-in-channel-flow model so that the measured stability boundaries are reproduced with the model. This dependence of the phase angle on the reduced gap velocity can be approximated by an exponential function, see Fig. 18. Using the approximation of the phase angle the stability diagram in Fig. 19 is obtained where the axes are interchanged compared to the usual representation. The unstable region is situated below the stability boundary. From the mechanical point of view only mass-damping parameters $\delta_r \geqslant 0$ are significant. For reduced gap velocities $V_r \leqslant 30$ the two hatched regions with unstable behavior are found. Similar to the experimental investigations of one single flexible tube in Fig. 1 multiple stability boundaries are found, i.e., when the reduced gap velocity is varied at a constant mass-damping parameter the stability boundary is intersected more than once.

A possible explanation for the stabilization of the tube due to increased upstream turbulence can be derived from a quasi-stationary approach for the tube damping, based on the results presented above. Eq. (22) characterizes a linearized system, the net damping of which consists of the structural damping and a fluid damping term. The quasi-stationary approach is made up of the assumption that the system with a time-dependent turbulent flow velocity always behaves as if the momentary flow velocity was constant. Actually this is only correct for a flow velocity that is fluctuating very slowly. Then, the stabilizing effect of the disturbed flow velocity can be explained by means of Fig. 20, where an enlarged part of Fig. 19 is shown. The horizontal line indicates an assumed positive mass-damping parameter $\delta_{r,st}$ of the structure. The corresponding reduced gap velocity of the upper stability boundary is $\bar{V}_r$. When the reduced gap velocity is reduced by a value V_r' the total system with the mass-damping parameter $\delta_{r,st}$ becomes unstable. The difference between the stability boundary and the mass-damping parameter $\delta_{\mathrm{res}}(\bar{V}_r - V_r')$ can be interpreted as a measure for the resulting negative net damping of the total system. On the other hand, if the reduced gap velocity is enhanced by a value V_r' the total system goes into the stable region and the difference between the stability boundary and the mass-damping parameter $\delta_{\mathrm{res}}(\bar{V}_r + V_r')$ can be understood as a measure for the resulting positive net damping of the total system. Here, it is obvious that the positive damping has the higher absolute value, which leads to an averaged stabilization, because in a normal distributed turbulent flow velocity negative and positive fluctuations occur with the same probability.

Finally, the mass-damping parameter of an averaged stability boundary for a fluctuating flow velocity can be computed by

$$\delta_r(\bar{V}_r, \mathrm{Tu}) = \int_{-\infty}^{\infty} \delta_r(V_r, \mathrm{Tu} = 0)\, p(V_r, \mathrm{Tu})\, \mathrm{d}V_r. \tag{23}$$

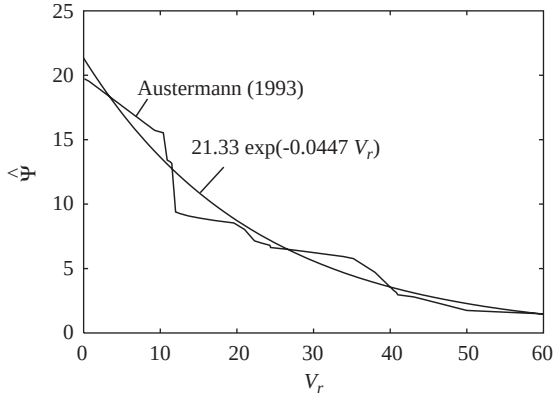

Fig. 18. Phase angle from Austermann (1993) and approximation.

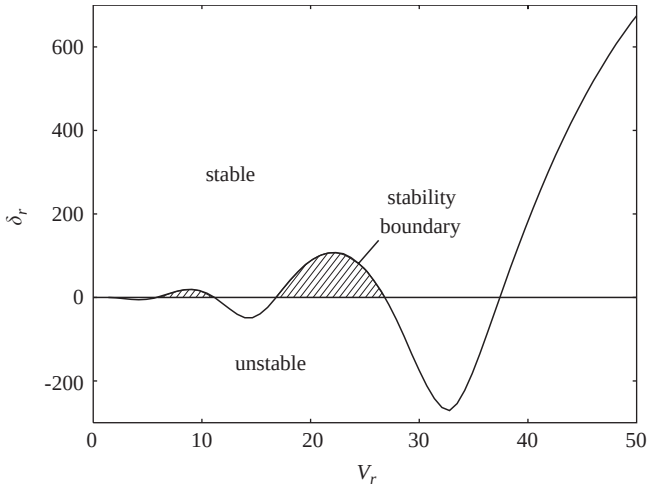

Fig. 19. Stability diagram of the tube-in-channel-flow model.

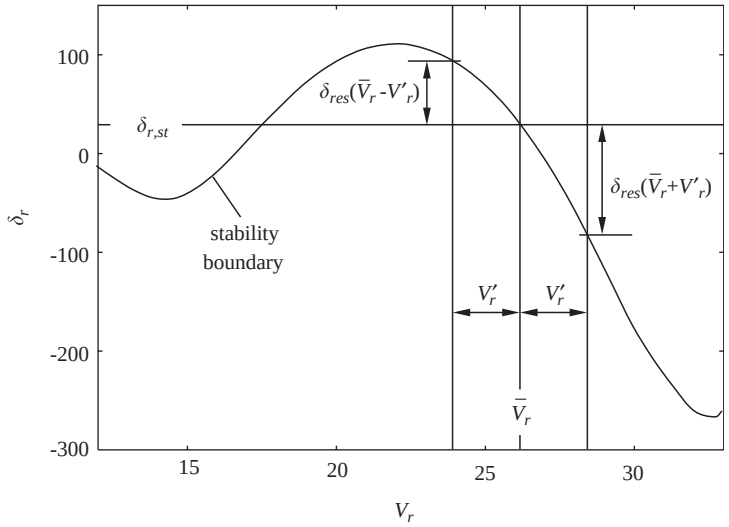

Fig. 20. Stabilization due to velocity perturbations.

Here, the function $\delta_r(V_r, \mathrm{Tu} = 0)$ represents the stability boundary of the tube-in-channel-flow model, cf. Fig. 19, and $p(V_r, \mathrm{Tu})$ is the probability density function of the normal distributed turbulent flow velocity.

This yields the stability diagram in Fig. 21 for different turbulence intensities between $0 \leqslant \mathrm{Tu} \leqslant 20\%$. For small mass-damping parameters δ_r the upper stability boundaries move to smaller reduced gap velocities V_r with increasing turbulence intensity, whereas the influence on the lower stability boundary is rather small. Furthermore, the mass-damping parameter which is needed for the stability of the system in the entire region of the reduced gap velocity decreases with increasing turbulence intensity, so that a complete stabilization is possible for certain mass-damping parameters. These tendencies qualitatively agree very well with the experimental observations. As one part of the explanation of the observed effects, higher flow velocities can be mentioned, which occasionally occur in the turbulent flow and lead to a high net damping.

7. Discussion of the theoretical results

The theoretical considerations are based on the tube-in-channel-flow model by Lever and Weaver (1982). The model itself rests on some intuitive assumptions and it is of course questionable, if the used quasi-stationary assumption is

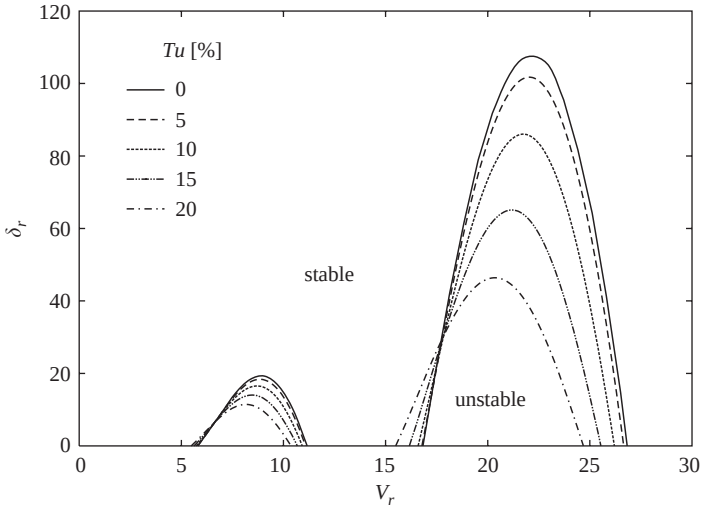

Fig. 21. Stability diagram for different turbulence intensities.

appropriate in the frequency range of the turbulent flow. However, none of the simple theoretical models, which have been published so far, could predict the influence of turbulence stability behavior correctly. In the theoretical studies of Lever and Rzentkowski (1989, 1998) an improvement of the stability behavior is not possible. Romberg (1998) theoretically considered the influence of turbulence by reducing the correlation length of the fluid force in the direction of the tube axis. Thus, a stabilizing effect of turbulence is achieved, but qualitatively there is no good agreement in the transition to stable behavior. However, using the quasi-stationary approach the mechanism can partly be explained and the stabilization observed experimentally can be reproduced qualitatively.

8. Conclusions

An experimental wind tunnel study of the effect of upstream turbulence on the stability behavior of a parallel triangular tube bundle ($P/d = 1.375$) has been carried out. For a single flexible tube in an otherwise fixed bundle a stabilizing effect has been shown already in former publications, cf. Romberg and Popp (1996) and Rottmann and Popp (2001). To make it more relevant for applications these investigations have been extended to bundles with various flexible tubes. The behavior of the flexible bundles is much more complex, but still for all investigated bundles a stabilizing effect of upstream turbulence was found. Compared to the behavior in smooth flow the critical reduced gap velocity could always be enhanced by at least 50%.

For practical use this means that stability problems in the first rows of specific arrays could be solved by providing a highly turbulent flow at the inlet. On the other hand, generating higher turbulence intensities could increase the buffeting amplitudes and, thereby, cause other problems that are not considered here. However, if the flow is already highly turbulent at the inlet of the bundle anyway, which is the case for many heat exchangers, the design recommendations derived from test tube bundles with low upstream turbulence might imply unexpected safety factors.

In the theoretical investigations for one flexible tube, based on the tube-in-channel-flow model, turbulence is considered by a quasi-stationary approach for the net damping of the tube, which depends on the flow velocity in smooth flow. With this approach a stabilization can be shown, which is similar to the experimental stabilization. Flow velocities beyond the upper stability boundary, which occasionally occur in the turbulent flow, yield high net damping coefficients, which result in an averaged stabilization. Thus, the observed effects can at least partly be explained.

References

Arnold, L., 1990. Stabilization by noise revisited. ZAMM 70, 235–246.

Austermann, R., 1993. Zum Schwingungsverhalten querangeströmter Rohrbündel bei Anregung vom Galloping-Typ. Ph.D. Thesis, University of Hannover, Institute of Mechanics (in German).

Austermann, R., Popp, K., 1995. Stability behavior of a single flexible cylinder in rigid tube arrays of different geometry subjected to cross-flow. Journal of Fluids and Structures 9, 303–322.

Baines, W.D., Peterson, E.G., 1951. An investigation of flow through screens. Transactions of the ASME 73, 467–480.

Bucher, C.G., Lin, Y.K., 1988. Stochastic stability of bridges considering coupled modes. ASCE Journal of Engineering Mechanics 114, 2055–2071.

Gorman, D.J., 1980. The effects of artificially induced up-stream turbulence on the liquid cross-flow induced vibration of tube bundles. In: M.K. Au-Yang, Flow-Induced Vibration of Power Plant Components, ASME PVP-41, ASME, New York, pp. 33–43.

Kassera, V., Strohmeier, K., 1997. Simulation of tube bundle vibrations induced by cross-flow. Journal of Fluids and Structures 11, 909–928.

Landahl, M.T., Mollo-Christensen, E., 1992. Turbulence and Random Processes in Fluid Mechanics, 2nd Edition. Cambridge University Press, Cambridge, MA.

Lever, J.H., Rzentkowski, G., 1989. Determination of the fluidelastic stability threshold in the presence of turbulence: a theoretical study. ASME Journal of Pressure Vessel Technology 111, 407–419.

Lever, J.H., Rzentkowski, G., 1998. An effect of turbulence on fluidelastic instability in tube bundles: a nonlinear analysis. Journal of Fluids and Structures 12, 561–590.

Lever, J.H., Weaver, D.S., 1982. A theoretical model for fluidelastic instability in heat exchanger tube bundles. ASME Journal of Pressure Vessel Technology 104, 147–158.

Lever, J.H., Weaver, D.S., 1986. On the stability of heat exchanger tube bundles, part I: modified theoretical model. Journal of Sound and Vibration 107, 375–392.

Price, S.J., 1995. A review of theoretical models for fluidelastic instability of cylinder arrays in cross-flow. Journal of Fluids and Structures 9, 463–518.

Romberg, O., 1998. Zum Turbulenzeinfluß auf das Schwingungsverhalten querangeströmter Rohrbündel. Ph.D. Thesis, University of Hannover, Institute of Mechanics (in German).

Romberg, O., Popp, K., 1996. The influence of upstream turbulence on the stability of tube bundles subjected to cross-flow. In: M. Pettigrew, Flow-Induced Vibration-1996, PVP-Vol. 328. ASME, NY, USA, pp. 11–18.

Rottmann, M., Popp, K., 2001. Experimental and theoretical investigations of the influence of upstream turbulence on the stability boundaries of a single flexible tube in a bundle. In: M. Pettigrew, Flow-Induced Vibration-2001, PVP-Vol. 420-1. ASME, NY, USA, pp. 109–116.

Rzentkowski, G., Lever, H.J., 1992. Modelling the nonlinear fluidelastic behavior of a tube bundle. In: M.P. Païdoussis, S.S. Chen, D.A. Steininger, Cross-Flow Induced Vibration of Cylinder Arrays, PVP-Vol. 242-2. ASME, NY, USA, pp. 89–106.

Schröder, K., Gelbe, H., 1999. New design recommendations for fluidelastic instability in heat exchanger tube bundles. Journal of Fluids and Structures 13, 361–379.

Soper, B.M.H., 1982. The effect of grid generated turbulence on the fluidelastic instability of tube bundles in cross-flow. In: Taborek, J., Hewitt, G.F., Afgan, N. (Eds), Heat Exchangers: Theory and Praxis. Hemisphere Publishing Corporation, Washington, pp. 325–337.

Southworth, P.J., Zdravkovich, M.M., 1975. Effect of grid turbulence on the fluidelastic vibrations of in-line tube banks in cross-flow. Journal of Sound and Vibration 39, 461–469.

Weaver, D.S., Fitzpatrick, J.A., 1988. A review of flow induced vibrations in heat exchangers. Journal of Fluids and Structures 2, 73–93.

Weaver, D.S., Fitzpatrick, J.A., ElKashlan, M., 1986. Strouhal numbers for heat exchanger tube arrays in cross flow. Proceedings of The Pressure Vessels and Piping Conference and Exhibition, Chicago, PVP-Vol. 104. American Society for Mechanical Engineers, NY, USA, pp. 193–200.